



Research Article

Long-term flare energy variation driven by the dipole moment of solar magnetic field

Ezgi Yoldaş and Hasan Ali Dal

Department of Astronomy and Space Sciences, Science Faculty, Ege University, Bornova, İzmir, Turkey

Abstract

In this study, the results obtained using GOES satellite X-ray data and MWO and WSO measurements of the solar magnetic field between 1976 and 2022 are compared and discussed. By analysing GOES satellite X-ray data in 47 different time periods of one month long, 7 500 solar flares are obtained, the flare equivalent duration distributions against the total duration of the flare are statistically modelled, and then their variation via time is examined. The variations of the model parameters such as the *Plateau*, which is considered as an indicator of the stellar saturation level in an observation season, and the flare timescales via time are examined. We noticed that the variation found in the solar magnetic field and the variation determined in the flare saturation levels are very similar. As a result, it is well known that the solar magnetic dipole moment measured from the solar poles steadily decreased from 1976 to 2022. We revealed that the solar X-ray flare energies are also generally decreasing in the same trend. This decrease is also evident in flare timescales, indicating that the geometry of solar magnetic loops is getting smaller over time.

Keywords: Techniques: photometric; methods: data analysis; methods: statistical; Sun: activity; Sun: flares; Sun: X-rays; gamma rays

(Received 27 March 2024; revised 13 November 2024; accepted 18 November 2024)

1. Introduction

Solar activity is a general term, which describes the structures that arise as a result of the interaction of the locally collected magnetic field with the plasma. The most common activity indicators are sunspots and flares. Although the oldest records of sunspots were found in Chinese sources dating back 2 000 yr (Clark & Stephenson 1978; Wittmann & Xu 1987), the first observation of sunspots was made by Galileo Galilei in 1610. The solar flare structures were first detected by Carrington (1859) and Hodgson (1859) on September 1, 1959. Flares are eruptive structures that occur with the sudden and intense release of magnetic energy stored in solar active regions (Shibata & Yokoyama 2002; Gershberg 2005; Benz & Güdel 2010; Shibata & Magara 2011; Shibata et al. 2013; Shibayama et al. 2013).

Sunspots are considered the most important indicator of solar activity because sunspot data are covering a long time period (Hathaway 2010). It was first demonstrated by the German astronomer Schwabe in 1844 that sunspot numbers exhibit a cyclical behaviour lasting approximately 10 yr. The sunspot number is nowadays considered to exhibit a cyclical behaviour with a period of approximately 11 yr (Schwabe 1844; Arlt 2011; van Driel-Gesztelyi & Owens 2020). It is accepted that the solar activity cycle is triggered by dynamo processes and plasma movements surrounding the boundary layer just below the solar convection zone, known as the tachocline (Gilman 2000, 2020; Weiss & Tobias 2000; Ghizaru, Charbonneau, & Smolarkiewicz 2010;

Bertello, Pevtsov, & Ulrich 2020). In a solar cycle, the surface magnetic fields appearing around the latitudes of 45 degrees migrate towards the equatorial field. This migration movement changes the polarity of the solar poles' magnetic field every 11 yr and both hemispheres get opposite poles (Mursula & Ulich 1998).

The solar flare number variation over time correlates well with the sunspot number variation as well as other activity indicators (Hathaway 2015). The general impression is that strong flares come at the maximums of the solar cycles. However, since the Geostationary Orbital Environmental Satellites (GOES) began collecting data in 1975, it was noticed that active regions that produce strong flares can be seen at any stage of the spot cycle, including cycle minima (White et al. 2005; Motorina et al. 2020). Typical solar flare energies range from 10^{28} to 10^{33} erg (Schrijver et al. 2012; Aulanier et al. 2013). However, in recent years, an extremely surprising finding was made. Recent flare surveys of Sun-like active stars reveal that slowly rotating dwarfs from spectral types of G and K ($5\ 100\ \text{K} < T_{\text{eff}} < 6\ 000\ \text{K}$ and $\log g > 4.0$) can exhibit superflares (Schaefer, King, & Deliyannis 2000; Maehara et al. 2012). It is still unclear whether such superflares, whose energies are between 10^{33} – 10^{38} erg can also occur on the Sun (Berdyugina 2005; Strassmeier 2009; Aulanier et al. 2013).

This situation is surprising because magnetic activity is directly related to the evolutionary state of a star. Stars exhibiting flare activity appear to be either very young stars that have just arrived in the main sequence, or pre-main sequence stars, which are about to arrive in the main sequence. (Skumanich 1972) indicated that the stellar rotation speed decreases by increasing stellar age. In this case, a young star has a very high rotation speed, which makes the magnetic activity increase. However, the magnetic activity level depends not only on the stellar rotation

Corresponding author: Hasan Ali Dal; Email: ali.dal@ege.edu.tr

Cite this article: Yoldaş E and Dal HA. (2024) Long-term flare energy variation driven by the dipole moment of solar magnetic field. *Publications of the Astronomical Society of Australia* 41, e113, 1–13. <https://doi.org/10.1017/pasa.2024.120>

speed but also on the depth of the stellar convection zone (Gershberg 2005).

Determining the saturation level of flare activity exhibited by stars from different spectral types is important in terms of determining the maximum flare energies that can be observed within the cyclic nature of the activity in that spectral type. Different saturation definitions can be made regarding the upper limit values of different parameters that characterise a flare event. The saturation level of a flare event can be defined for different parameters, such as the upper limit of magnetic field intensity, the upper limit of electron density, or the upper limit of flare loop temperature. In this study, the saturation level is defined as an average maximum flare energy that is observed in a star. However, determining the saturation level is a difficult and still controversial issue. Yoldaş & Dal (2016, 2017, 2021), Dal & Yoldaş (2023), who have conducted studies on the flare activity exhibited by the stars from K and M spectrum types in recent years, developed a model called as ‘One Phase Exponential Association model’ (hereafter OPEA) to determine the white light flare saturation levels of an individual star and so its flare activity behaviour. Recently, they applied this model to solar flares, by using the X-ray data, too (Yoldaş & Dal 2022, 2023). The OPEA is an exponential model of the equivalent duration distribution via flare total duration calculated for the flares detected on an individual star, which indicates that this distribution varies in a certain rule. The most important parameter of this model is the Plateau value, which is defined as the saturation level for flare activity in the observed wavelength range (Dal & Evren 2010, 2011).

Examining the variations in solar flare energies over time, the authors reached some findings contrary to the Solar Activity Cycle. In this study, considering that the Sun is a single star and there could be no major variations in its internal structure within a few decades, the magnetic field effects are examined as the cause of the variation obtained for limited observation time intervals by Yoldaş & Dal (2022, 2023).

The solar near-polar magnetic field has been regularly measured with the required precision at Mount Wilson (MWO) since 1967 and at the Wilcox Solar Observatories (WSO) since 1976 (Ulrich et al. 2002; Svalgaard, Duvall, & Scherrer 1978). The Babcocks’ pioneering observations showed that the polar fields were very strong in 1952–1954, but then their polarity changed in 1957–1958 (Babcock & Babcock 1955; Babcock 1959). Scattered measurements in the 1960s confirmed that the polar fields reached maximum values at the sunspot minimum and the opposite sign at the sunspot maximum (Severny 1971). Svalgaard et al. (2005) showed that many solar cycles are characterised quite well by a single parameter. According to the authors, how a cycle takes shape directly depends on the behaviour and state of the Sun’s magnetic field in the previous cycle. On the other hand, while two of the eight strongest storms in the last 150 yr occurred during the 14th Solar Activity Cycle (Cliver & Svalgaard 2004), three of the five largest proton events with 30 MeV energy have occurred since 1859 occurred during the 13th Solar Activity Cycle (McCracken et al. 2001). On the other hand, Dikpati et al. (2004) suggest that the magnetic ‘memory’ of the Solar Activity Cycle is 17–21 yr, and thus the polar fields at the end of n^{th} cycle may have a strong correlation with the subsurface toroidal fields of the $(n + 2)^{\text{th}}$ cycle. Therefore, the unexpected variations revealed in the initial results obtained by Yoldaş & Dal (2022, 2023) depending on GOES X-ray data are similar to the findings of Svalgaard et al. (2005), Dikpati et al. (2004).

In this study, we discuss the behaviour of flare energy variation in the last five Solar Activity Cycles and its relationship with the Solar magnetic dipole moment variation. For this aim, data from the Geostationary Orbital Environmental Satellites (GOES) (White et al. 2005; Motorina et al. 2020) are used. Details about these data are presented in Section 2. WSO magnetic field measurement data^a are used for comparison with flare activity behaviour (Svalgaard et al. 2005). Details about these data are presented in Section 2, too. Details on how flares are detected from the data and how their parameters are calculated are given in Section 3. The details about the OPEA model and its parameters are given in Section 4, while the relationship between the magnetic field and the OPEA model is presented in Section 5. The results are discussed in Section 6.

2. Data sources

Geostationally Operational Environmental Satellites (GOES), whose main aim is to make continuous meteorological observations of the Earth, were first launched in 1975. In addition to this task, the X-ray detectors (XRS) mounted on these satellites continuously accumulated the fluxes from the Sun in the wavelength ranges of 0.5–4.0 Å (short channel, nearly hard X-ray) and 1.0–8.0 Å (long channel, almost soft X-ray). Regular observational data taken in hard and soft X-ray regions for approximately 46 yr have been published in public databases (www.goes.noaa.gov). The exposure times of the satellites were 3 s before 2009 and 2 s after that (Garcia 1994).

In this study, we do not make any frequency analysis for light variation, which is generally affected by exposure time variations. An analysis of the flare general light curve is performed, because of this, exposure time variation does not affect the analysis results. In the analysis, data accumulated by GOES satellites in the wavelength range of 0.5–4.0 Å (short channel) are used. The data are selected from 47 different time intervals distributed almost homogeneously along the 20th, 21st, 22nd, 23rd, 24th, and 25th Solar Activity Cycles. The time intervals selected for analysis are shown by filled big red circles in Fig. 1. As it is seen from the figure, although it was desirable to select evenly spaced time intervals, but this was not possible due to technical problems in the data obtained from the database. For this reason, the most homogeneous intervals that have no technical problems have been selected so that there is data at different phases of each cycle.

Long-term flare energy variation between the 20th and 25th Solar Activity Cycles is compared with the Sun’s magnetic dipole moment variation. For this comparison, MWO and WSO magnetic field measurements are used. MWO and WSO measurements show the same behaviour. The instruments and measurement details of WSO (<http://quake.stanford.edu/wso/Polar.ascii>) have not changed significantly over the decades. The solar disc image is scanned with a square aperture of 175 arcsec \times 175 arcsec in sky plane. This is very good resolution in view field, considering the solar radius is about 1 000 arcsec. The line-of-sight component of the magnetic field is measured using the Fe I (λ 5 250 Å) line. The typical error in measurements is about 5 μ Tesla (Svalgaard et al. 2005). WSO data are prepared as 30-day averages of the magnetic field measured, and these averages are calculated every

^a<http://quake.stanford.edu/wso/Polar.ascii>.

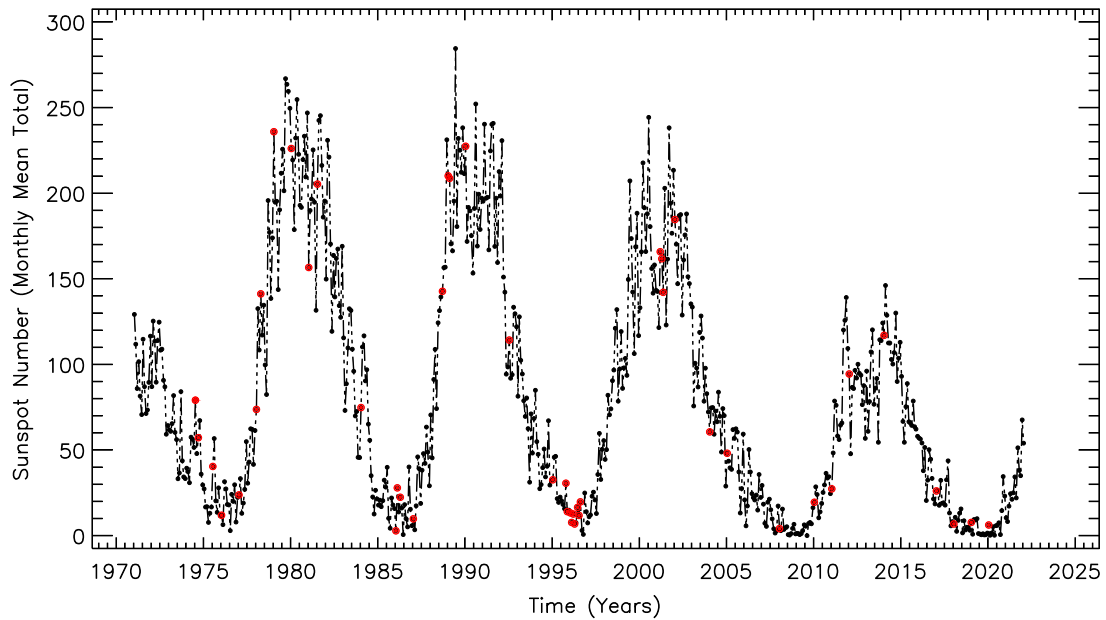


Figure 1. The variation in sunspot numbers between 1965 and 2022, from the beginning of the 20th Sunspot Cycle to the first years of the 25th cycle, created with data taken from the SOHO database. The small filled black circles show the monthly average spot numbers, while the big filled red circles represent the months for which OPEA models were created.

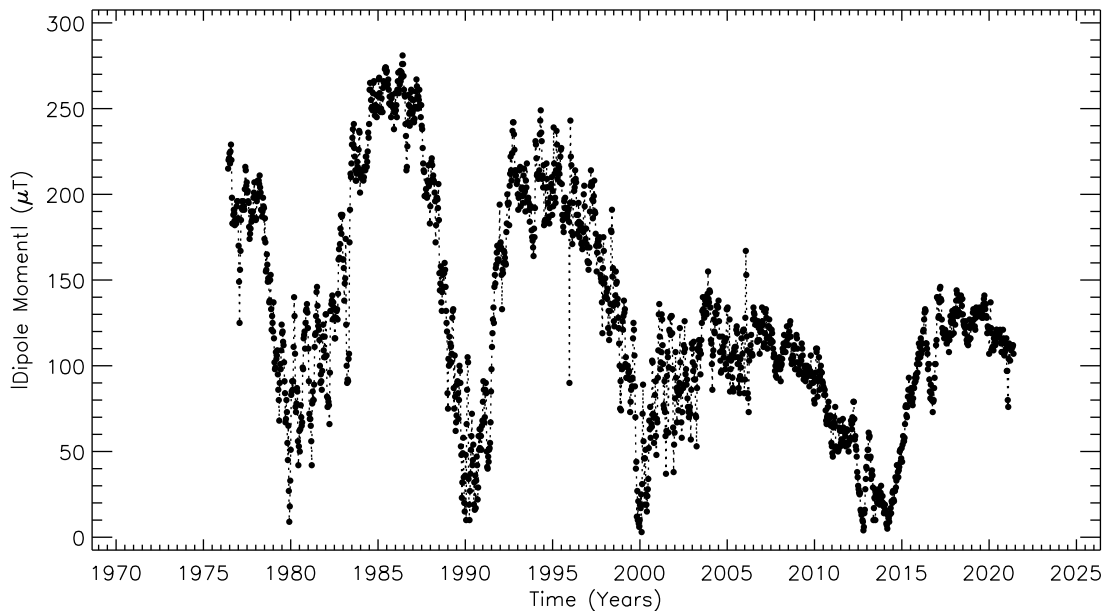


Figure 2. The variation in the absolute dipole moment ($|DM|$) in units of micro Tesla (μT) computed by using the magnetic field measured from the Sun’s geographical latitude intervals between $+55^\circ / +90^\circ$ North latitudes and $-55^\circ / -90^\circ$ South is shown.

10 days. Following Svalgaard et al. (2005), the dipole moment ($|DM|$) studied in this paper is defined as the difference between the average unsigned polar fields in the North and in the South and is computed using magnetic field measurements from WSO. Fig. 2 shows the time variation of the $|DM|$ values over three solar cycles, between 1970 and 2020. MWO data were measured every 10 days from the area matching WSO measurements and archived

as the average of measurements taken along 30 days (Svalgaard et al. 2005).

3. Flare detection and calculation of parameters

We used the method, whose details are given by Dal (2020), to detect flares in the solar data taken from the GOES database and

calculate the flare parameters. The flare quiescent level, the flare rise time, and the flare decay time were defined using three different polynomial functions that fit the three parts of the flare light curve with the least squares method. A linear function (e.g. $f_1(x)$ function) was used for the flare quiescent level, while second or third-degree functions were used for the flare rise (e.g. $f_2(x)$ function) and flare decay (e.g. $f_3(x)$ function) depending on the correlation coefficients of the fits. In the calculations, the intersection point of the $f_1(x)$ and $f_2(x)$ functions was taken as the flare start point, the intersection point of the $f_2(x)$ and $f_3(x)$ functions as the flare maximum point, and the intersection point of the $f_3(x)$ and $f_1(x)$ functions as the flare endpoint. In addition, we also calculated the uncertainties in finding these points, which were then used to compute the uncertainties in the flare timescales.

After the flare beginning and end times are determined for all flares, flare rise (T_r) and decay (T_d) times, flare amplitude, and equivalent duration (P) are calculated. The averaged amplitude of the fluctuations in the quiescent period outside the flare is accepted as an observation error (σ). If the brightness in the light curve begins to increase and its amplitude reaches above 3σ , this is considered a flare. Considering the flare beginning, maximum and end times, the duration between the flare beginning and maximum is defined as the flare rise time (T_r), and the duration between the flare maximum and end is defined as the flare decay time (T_d). The sum of these two durations is defined as the flare total time (T_t). On the other hand, the equivalent duration of a flare is calculated with Equation (1) defined by Gershberg (1972):

$$P = \int [(I_{flare} - I_0)/I_0] dt \quad (1)$$

where P is the flare equivalent duration in seconds, I_{flare} is the flux at the moment of a flare, and I_0 is the quiescent level flux. The least squares method is used in all the calculations. The important point to remember here is that calculations are made separately for each flare. The integral in Equation 1 is conducted between the starting and ending times of the flare burst. The time interval dt for each flare varies because the total duration of each flare varies. In the calculations, I_{flare} is calculated using $f_2(x)$ and $f_3(x)$ functions for the flare duration, while the I_0 is computed by the $f_1(x)$ function.

Between the years 1964 and 2022, we detected 7 500 flares in 47 separate time intervals of one month each. Then, statistical models are carried out on all flare parameters. Statistical studies are carried out in two ways. First, each monthly data is analysed on its own, and then the data in each activity cycle interval is analysed, considering the start and end dates of the Solar Activity Cycles given in the literature.

4. Calculation of OPEA model and parameters

When the relations between the flare parameters are examined, it is seen that the flare equivalent time varies versus the total flare time according to a certain rule, as in the similar examples in the literature (Dal & Evren 2011; Dal 2020; Yoldaş & Dal 2022, 2023). Using the regression calculations carry out with the SPSS V17.0 (Green et al. 1996) and Grahpad Prism V5.02 (Dawson & Trapp 2004) programmes, we show that the best model function for the flare equivalent time distribution versus the total flare time is the One Phase Exponential Association (hereafter, OPEA). The OPEA function is a special function with having the *Plateau* term, which

is defined by Equation (2) (Motulsky 2007; Spanier & Oldham 1987):

$$y = y_0 + (Plateau - y_0) \times (1 - e^{-k \times x}) \quad (2)$$

In the first step, the OPEA models are derived depending on the flares obtained in each selected monthly period. Then, the OPEA models are separately derived from the flares detected in each cycle interval. During these modelling, three separate statistical probability are calculated to test whether the distributions obtained in each data set could be modelled with another function except the OPEA function. These tests are the D'Agostino-Pearson normality test, the Shapiro-Wilk normality test and also the Kolmogorov-Smirnov tests (D'Agostino & Stephens 1986). Considering all these tests, we found as a *p-value* < 0.001 in all cases. This result showed that each distribution can be best represented by OPEA model and cannot be fitted by any other function (Motulsky 2007; Spanier & Oldham 1987).

The parameters of y_0 , *Plateau*, *k*-value, etc., are determined from the model fit. If we consider the mathematical definition of the model function, y_0 is the value of the model at the point where it intersects the *y*-axis. *Plateau* is the highest *y*-value that the model can take. The *k*-value and *Tau*-value are the constant coefficient for that model. According to Motulsky (2007), *k*-value is the rate constant, expressed in reciprocal of the *x*-axis time units, while *Tau*-value is the time constant, expressed in the same units as the *x*-axis. It is computed as the reciprocal of *k*-value. All these parameters, which are adjustable parameters of the model function, are variable for different models. According to Yoldaş & Dal (2022, 2023), here *y* is the equivalent duration on a logarithmic scale, *x* is the flare total time, and y_0 is the flare equivalent duration on a logarithmic scale for the minimum flare total time. In other words, y_0 defines the minimum equivalent duration for a flare to be able to observed in a star. The *Plateau* value defines the upper limit of the equivalent duration for the flares observed on an individual star. This parameter is defined as the saturation level for flare activity in the observed wavelength range (Dal 2020).

The model parameters obtained for each one-month time interval are listed in Table 1. In the table, the midpoint times of the selected one-month time intervals are listed in the first column, while y_0 , *Plateau*, *K*, *Tau*, *Half - Time*, and the *span* values are tabulated in the following column with their errors, respectively. In the last column, the number of flares obtained for that period are listed. When the variations of all these parameters are examined over time, it is seen that both y_0 and *Plateau* parameters follow two different trends. First of all, both parameters decrease with time linearly. Moreover, it is also seen that both parameters exhibit a vaguely sinusoidal variation apart from this linear trend. These variations are surprising because both of them have a different variation character comparing to the Solar Activity Cycle. These variations are shown in the top panel of Fig. 3.

The *Span* value is the difference between the *Plateau* and y_0 values. In short, the *Span* value is an indicator of the difference in the equivalent durations of the largest and smallest flare energies. As seen in the bottom panel of Fig. 3, if the variation of *Span* value via time is carefully examined, it is seen that it shows a decreasing trend over time. This is another surprising finding.

Another parameter is the *Half - Time* that is computed as *Half - Time* = $\ln 2/k$. It is theoretically assumed that *Half - Time* is a half of the total duration for a flare that is the first flare, whose equivalent duration firstly reaches the *Plateau* level. In another

Table 1. The parameter list of 47 separate OPEA models created with X-ray data in the wavelength range 0.5–4.0 Å (short channel) taken from the GOES database.

Year	y_0 (s)	Plateau (s)	k (s ⁻¹)	τ (s)	Half – time (s)	Span (s)	N_{flare}
1974.53700	3.512 ± 0.101	7.258 ± 0.193	0.00033 ± 0.00004	3 071.61	4 129.08	3.747 ± 0.190	119
1974.53700	2.960 ± 0.406	5.593 ± 0.496	0.00037 ± 0.00013	2 687.00	1 863.00	2.633 ± 0.515	14
1974.70680	3.432 ± 0.212	7.018 ± 0.188	0.00035 ± 0.00006	2 885.00	4 000.00	3.586 ± 0.263	41
1975.53700	2.658 ± 0.306	4.966 ± 0.249	0.00067 ± 0.00039	1 482.80	1 027.80	2.308 ± 0.207	26
1976.04110	2.685 ± 0.126	4.939 ± 0.067	0.00060 ± 0.00008	1 676.10	1 161.78	2.254 ± 0.125	71
1977.04110	2.832 ± 0.159	5.211 ± 0.042	0.00062 ± 0.00009	1 612.48	1 117.69	2.379 ± 0.157	75
1978.28770	2.746 ± 0.073	5.949 ± 0.192	0.00014 ± 0.00002	7 060.05	4 893.65	3.203 ± 0.177	366
1979.04110	3.072 ± 0.077	5.611 ± 0.183	0.00023 ± 0.00004	4 271.92	2 961.07	2.539 ± 0.163	502
1980.04110	3.102 ± 0.063	6.486 ± 0.385	0.00011 ± 0.00002	8 735.71	6 055.13	3.384 ± 0.360	396
1981.04110	2.738 ± 0.158	4.804 ± 0.164	0.00030 ± 0.00007	3 297.70	2 285.79	2.066 ± 0.153	192
1981.53700	2.576 ± 0.085	5.635 ± 0.191	0.00030 ± 0.00004	3 370.47	2 336.23	3.059 ± 0.169	213
1984.04110	2.701 ± 0.056	4.979 ± 0.119	0.00025 ± 0.00003	3 976.24	2 756.12	2.278 ± 0.107	360
1986.04110	2.791 ± 0.147	5.212 ± 0.192	0.00022 ± 0.00005	4 488.54	3 111.22	2.422 ± 0.201	69
1986.12600	2.903 ± 0.053	6.145 ± 0.156	0.00014 ± 0.00001	7 268.55	5 038.18	3.242 ± 0.150	204
1986.28770	2.429 ± 0.115	5.156 ± 0.457	0.00034 ± 0.00011	2 928.04	2 029.56	2.727 ± 0.402	98
1987.04110	2.282 ± 0.373	4.224 ± 0.258	0.00120 ± 0.00059	835.59	2 579.18	1.941 ± 0.314	35
1988.70960	2.765 ± 0.070	5.325 ± 0.144	0.00019 ± 0.00002	5 135.37	3 559.57	2.560 ± 0.129	320
1989.04110	2.423 ± 0.086	5.382 ± 0.117	0.00015 ± 0.00002	6 762.94	4 687.71	2.959 ± 0.109	338
1989.12600	2.610 ± 0.063	5.592 ± 0.142	0.00013 ± 0.00001	7 868.31	5 453.90	2.983 ± 0.127	340
1990.04110	2.257 ± 0.076	4.833 ± 0.092	0.00039 ± 0.00004	2 544.83	1 763.95	2.577 ± 0.092	354
1992.53970	2.933 ± 0.119	5.301 ± 0.174	0.00019 ± 0.00004	5 265.39	3 649.69	2.368 ± 0.160	237
1995.04110	3.206 ± 0.078	5.856 ± 0.183	0.00024 ± 0.00004	4 148.04	2 875.20	2.649 ± 0.164	177
1995.78900	3.094 ± 0.127	5.728 ± 0.257	0.00026 ± 0.00006	3 794.86	2 630.40	2.634 ± 0.237	104
1995.87400	2.374 ± 0.170	5.045 ± 0.233	0.00081 ± 0.00019	1 232.55	854.34	2.670 ± 0.229	39
1996.04110	2.821 ± 0.197	4.604 ± 0.136	0.00087 ± 0.00022	1 146.46	794.67	1.783 ± 0.158	52
1996.12600	2.033 ± 0.409	4.829 ± 0.063	0.00639 ± 0.00235	156.45	108.45	2.795 ± 0.398	16
1996.20550	1.860 ± 0.343	4.575 ± 0.086	0.00190 ± 0.00037	525.72	364.40	2.715 ± 0.335	31
1996.29040	3.369 ± 0.228	5.160 ± 0.276	0.00025 ± 0.00011	3 991.38	2 766.61	1.792 ± 0.262	31
1996.45750	2.315 ± 0.530	4.353 ± 0.167	0.00146 ± 0.00061	682.85	473.32	2.037 ± 0.495	20
1996.53970	2.867 ± 0.112	5.685 ± 0.311	0.00019 ± 0.00004	5 256.33	3 643.41	2.818 ± 0.280	91
1996.62470	1.839 ± 0.967	4.430 ± 0.111	0.00118 ± 0.00041	845.71	586.20	2.591 ± 0.926	28
2001.20270	3.026 ± 0.124	5.053 ± 0.110	0.00030 ± 0.00005	3 341.46	2 316.12	2.027 ± 0.126	225
2001.28770	2.545 ± 0.064	5.676 ± 0.138	0.00017 ± 0.00002	5 724.02	3 967.59	3.131 ± 0.130	401
2001.36990	2.697 ± 0.058	5.338 ± 0.080	0.00025 ± 0.00002	3 975.57	2 755.66	2.640 ± 0.079	388
2002.04110	2.811 ± 0.096	5.271 ± 0.097	0.00015 ± 0.00002	6 581.60	4 562.01	2.460 ± 0.103	301
2004.04110	2.093 ± 0.141	5.140 ± 0.181	0.00022 ± 0.00003	4 641.86	3 217.49	3.047 ± 0.185	136
2005.04110	2.923 ± 0.084	6.465 ± 0.213	0.00007 ± 0.00001	14 641.70	4 148.80	3.542 ± 0.208	156
2008.04110	2.527 ± 0.162	4.633 ± 0.104	0.00021 ± 0.00004	4 751.46	3 293.46	2.106 ± 0.169	39
2010.04110	2.852 ± 0.067	5.501 ± 0.096	0.00047 ± 0.00005	2 116.54	2 467.08	2.650 ± 0.094	161
2011.04110	2.171 ± 0.219	4.948 ± 0.122	0.00114 ± 0.00017	880.09	2 610.03	2.777 ± 0.226	55
2012.04110	3.216 ± 0.056	5.937 ± 0.093	0.00027 ± 0.00002	3 642.35	2 524.69	2.721 ± 0.093	289
2014.04110	3.074 ± 0.108	5.614 ± 0.187	0.00015 ± 0.00003	6 791.83	4 707.74	2.540 ± 0.163	246
2017.04110	2.525 ± 0.177	5.051 ± 0.104	0.00025 ± 0.00005	4 064.18	2 817.07	2.526 ± 0.168	63
2018.04110	1.884 ± 0.175	3.842 ± 0.154	0.00032 ± 0.00009	3 166.89	2 195.12	1.958 ± 0.197	14
2019.04110	1.445 ± 0.279	4.012 ± 0.096	0.00057 ± 0.00010	1 765.78	1 223.95	2.566 ± 0.274	24
2019.04110	1.286 ± 0.091	3.571 ± 0.049	0.00045 ± 0.00004	2 246.43	1 557.11	2.285 ± 0.087	26
2020.04110	1.712 ± 0.105	4.242 ± 0.079	0.00008 ± 0.00001	13 231.20	2 171.14	2.530 ± 0.096	17

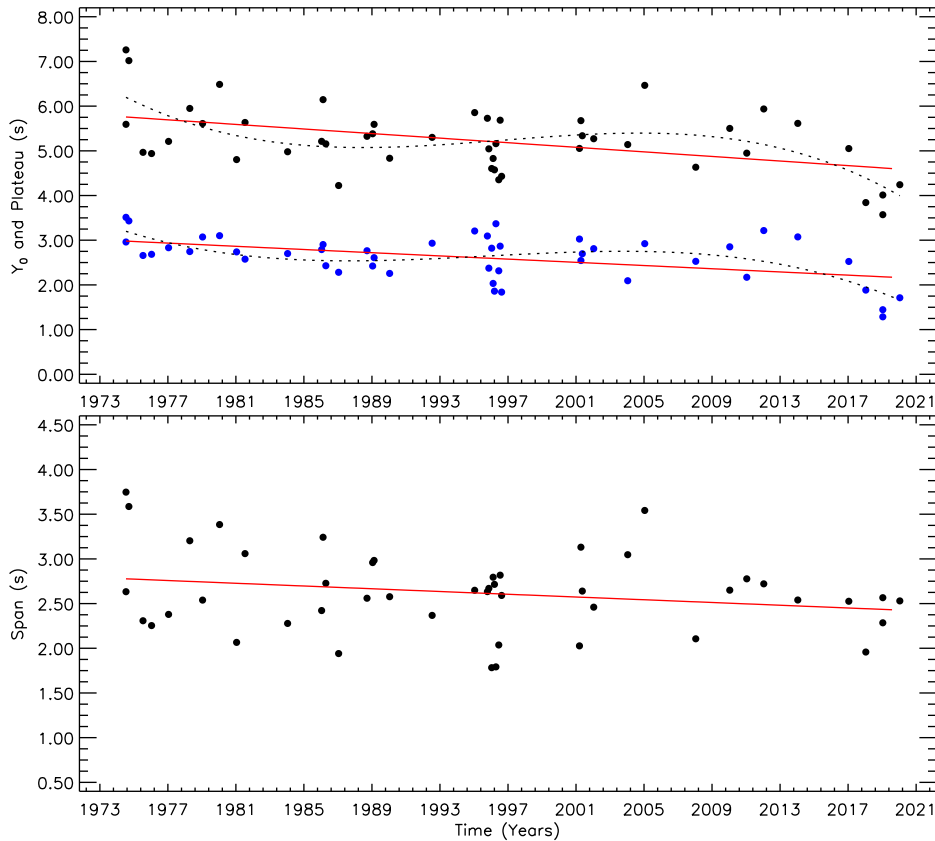


Figure 3. The variations of the basic model parameters such as *Plateau* and y_0 , and the *Span* value, which is the difference between them, are shown versus time by taking into account 47 different OPEA models derived by the flare data from 47 homogeneously selected one-month time intervals between 1974 and 2022. In the figures, the straight lines show the linear fits, while the dotted lines represent the 3-degree polynomial fits used to be able to indicate the variation seen out of linear trend.

words, *Half – Time* is the the smallest x -value, for which the $y - y_0$ reached the half of *Plateau* – y_0 . If the *Half – Time* parameter variation via the *Plateau* is considered, it is seen from Fig. 4, the *Half – Time* parameter increases in a linear trend by increasing *Plateau* parameter.

For each of the flare sets from which an OPEA model was created, we record the maximum rise time (T_r^{\max}), the maximum decay time (T_d^{\max}), and the maximum total duration (T_t^{\max}) of the flares in this set. These three parameters for all the flare sets are listed in Table 2, and are also plotted in Fig. 5. Each flare has three timescales determined from the observed light curve: flare rise time (T_r), flare decay time (T_d), and the total flare duration (T_t), which is the sum of the rise and decay times. Thus, the relationship between these three can be defined as $T_t = T_r + T_d$. However, a careful examination of the timescales listed in Table 2 reveals that the sum of the flare rise and decay times does not equal the corresponding total flare duration provided in the table. This discrepancy should not be misleading. The values listed in the table are derived from different flares in the flare data sets. In a given flare set, the rise time of one flare may represent the longest rise time, while the decay time of another flare in the same set may represent the longest decay time. The total flare duration can arise from any of these flares. Therefore, each row in the table represents the situation across different flare sets. The flare rise time in one row may belong to one flare, and the flare decay time to

another flare. As such, their sum may not correspond to the total flare duration in that row.

As it is seen in the upper panel of Fig. 5, the T_t timescale varies via the *Plateau* value that the T_t values increases by the increasing *Plateau* values. Moreover, if the T_r and T_d timescales are compared, it is recognised from the lower panel of the figure that the T_r timescale increases with the increasing T_d timescale; $\log T_r$ and $\log T_d$ can be fitted by a linear function, and the slope of this linear trend is 0.537 ± 0.077 . Because of this, in the case of the short T_d times, the decay time is $\log T_d = 3.5$ for example, and the rise time is also $\log T_r = 3.5$. In the case of the long times, the rise time is about $\log T_r = 4.5$ for the flares with a decay time of $\log T_d = 5.25$.

5. OPEA model and dipole moment correlation

Using MWO and WSO magnetic field measurements taken from the 20th to 25th Solar Activity Cycles, the average magnetic dipole moments in the years for which the OPEA model is created are calculated. Using magnetic field measurements are taken from the regions between the Sun’s geographical $+55^\circ / +90^\circ$ North latitudes and $-55^\circ / -90^\circ$ South latitudes (Svalgaard et al. 2005). Firstly, the magnetic dipole moments variation via time are checked. Although this variation seen in Fig. 6 seems to follow the Solar Activity Cycle, a linear fit applied to the data indicates that it generally follows a trend with a decreasing slope.

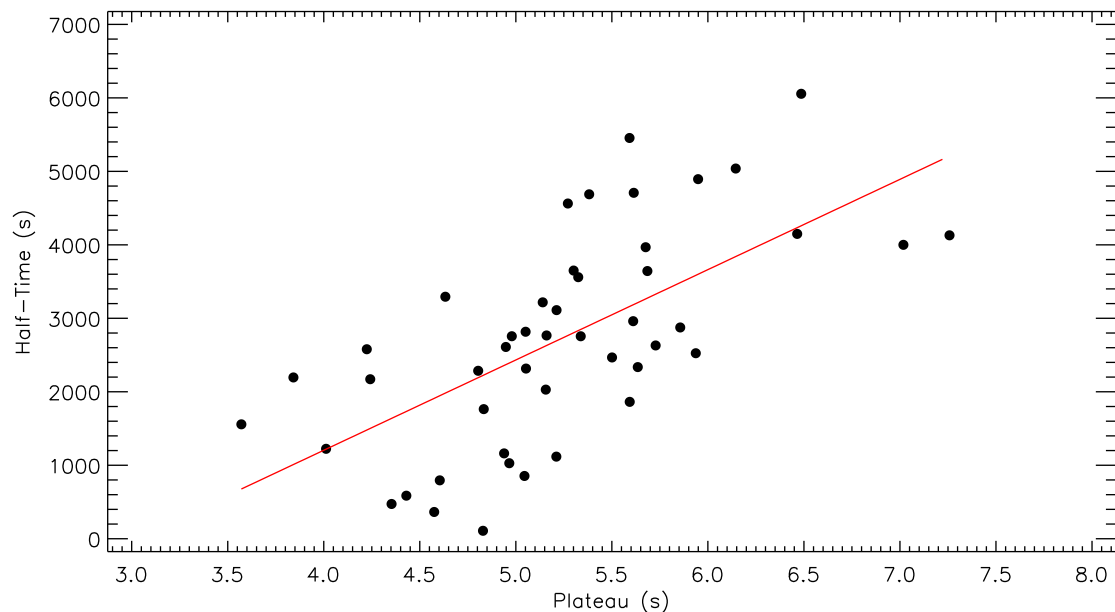


Figure 4. The *Half – Time* parameter variation versus the *Plateau* parameter obtained from 47 separate OPEA Models created with X-ray data in the 0.5–4.0 Å (short channel) wavelength range taken from the GOES database is shown. In the figure, the filled circles represent the timescales, while the straight line shows the linear fit.

The distribution pattern seen in Fig. 6 change when we use the monthly magnetic dipole moment averages by considering the months when the OPEA models were derived instead of annual averages. Although the variation via time in the monthly averages shown in Fig. 7 exhibits a linear trend with a decreasing slope, there is also an interesting situation here. If the monthly average dipole moment variations are fitted by a 3-degree polynomial rather than linearly as it is in the case of the *Plateau*, the 3-degree polynomial fit variations of both parameters form a mirror image of each other.

Here it must be noted that the variations of both parameters should be fitted by a sinusoidal function rather than a polynomial function, because the 3-degree polynomial function has not a physical meanings for these variations. However, there are not enough data to be able to obtain any sinusoidal function fit. This is why we had to choose the polynomial function to be able to indicate the variation seen out of linear trend.

On the other hand, this variation fitted by a 3-degree polynomial function manifests itself much more clearly with the magnetic measurements of the Sun obtained by indirect methods by van Driel-Gesztelyi & Owens (2020). When the cycle-to-cycle variation of the average Solar magnetic field measured separately during each Solar Activity Cycle is compared with the variation in the *Plateau* values obtained separately for each cycle, it is seen that they are perfect mirror images of each other. This result shown in Fig. 8 supports the finding obtained with monthly measurements and models.

Here, it should also be noted that we have not even reached the middle of the 25th Solar Activity Cycle, yet. Therefore, the last magnetic field measurement value are calculated based on data until 2022.

6. Results and discussion

The main purpose of this study is to reveal whether the OPEA model parameters change during the Solar Activity Cycles. First of all, according to Dierckx et al. (2013) and Shibayama et al. (2013), we expected that the *Plateau* parameter, which indicates the upper limit of the flare energy of OPEA models, would take low values at the minimum of a cycle and high values at the maximum. In fact, we want to reveal whether OPEA models would be copies of each other or exhibit a general characteristic change in successive activity cycles. If there is a change, we discuss the possible reasons for this change. When all analyses are completed, strong findings are obtained that there is a variation beyond our expectations.

6.1 Variation of OPEA model parameters via time

It is a well-known fact that the Sun exhibits 11-yr spot activity cycle. It is known that the number of solar flares exhibits increases and decreases over time and is in perfect correlation with the spot activity (Gershberg 2005; Benz & Güdel 2010; Hathaway 2015). Solar flares are divided into classes such as A, B, C, M, and X from low energy to high energy depending on their energy in the X-ray bands (Benz 2008). Although the flares can be observed at almost every energy level in all phases of a solar cycle, M and X class flares, especially X class, are observed at cycle maximums. The *Plateau* parameter is an indicator of the theoretical upper limit of a flare energy that can be observed in a star, which means that the flare with highest energies determine the *Plateau* level. Thus, M and X class flares in the monthly sets determine the *Plateau* level of OPEA model. This is why the *Plateau* levels should change at the minimum and maximum of the Solar Activity Cycles.

Table 2. List of longest flare timescales determined from the flare sets, from which 47 separate OPEA Models are derived by X-ray data in the 0.5–4.0 Å (short channel) wavelength range taken from the GOES database.

Time (Years)	T_r^{Max} (s)	T_d^{Max} (s)	T_t^{Max} (s)
1974.53699	7 617 ± 381	18 691 ± 769	22 895 ± 858
1974.53699	3 477 ± 87	10 623 ± 464	14 100 ± 472
1974.70685	6 242 ± 234	29 686 ± 453	31 157 ± 510
1975.53699	2 270 ± 28	3 275 ± 82	3760 ± 87
1976.04110	6 321 ± 137	8 527 ± 426	11 864 ± 448
1977.04110	7 538 ± 377	7 801 ± 390	12 351 ± 542
1978.28767	13 547 ± 316	131 317 ± 1398	139 452 ± 1 433
1979.04110	12 002 ± 750	15 761 ± 779	23 563 ± 1 082
1980.04110	32 973 ± 770	17 346 ± 618	34 446 ± 987
1981.04110	6 481 ± 243	13 537 ± 515	17 664 ± 570
1981.53699	4 416 ± 110	11 897 ± 544	14 637 ± 555
1984.04110	14 771 ± 308	16 156 ± 614	28 432 ± 687
1986.04110	11 327 ± 408	40 673 ± 643	52 000 ± 761
1986.12603	11 025 ± 389	60 868 ± 921	65 437 ± 1 000
1986.28767	3 223 ± 81	5 134 ± 193	6 674 ± 209
1987.04110	2 268 ± 28	2 540 ± 64	3 547 ± 70
1988.70959	10 355 ± 347	13 812 ± 536	20 819 ± 639
1989.04110	14 999 ± 325	53 481 ± 907	61 722 ± 964
1989.12603	14 192 ± 364	65 204 ± 1006	67 964 ± 1 070
1990.04110	11 487 ± 418	21 088 ± 372	26 073 ± 560
1992.53973	10 120 ± 433	130 438 ± 1215	132 350 ± 1 290
1995.04110	7 830 ± 392	15 991 ± 799	19 183 ± 890
1995.78904	10 110 ± 432	33 105 ± 793	35 737 ± 903
1995.87397	2 026 ± 25	6 805 ± 255	8 831 ± 256
1996.04110	3 238 ± 81	3 289 ± 82	4 241 ± 115
1996.12603	1 989 ± 25	2 129 ± 27	2 314 ± 36
1996.20548	7 666 ± 383	6 863 ± 257	14 529 ± 462
1996.29041	9 456 ± 473	12 332 ± 571	15 774 ± 741
1996.45753	2 335 ± 29	5 663 ± 212	7 998 ± 214
1996.53973	6 071 ± 228	11 676 ± 530	15 535 ± 577
1996.62466	8 109 ± 405	5 798 ± 217	13 907 ± 460
2001.20274	17 238 ± 508	19 137 ± 914	26 388 ± 1 046
2001.28767	13 452 ± 409	36 768 ± 894	43 590 ± 983
2001.36986	26 901 ± 699	32 718 ± 726	39 245 ± 1 007
2002.04110	67 029 ± 2 622	65 324 ± 1047	89 193 ± 2 824
2004.04110	15 159 ± 326	95 742 ± 974	110 900 ± 1 027
2005.04110	13 510 ± 513	145 377 ± 1416	150 234 ± 1 506
2008.04110	16 610 ± 453	48 330 ± 1083	64 077 ± 1 174
2010.04110	10 887 ± 480	7 498 ± 281	16 024 ± 557
2011.04110	2 964 ± 74	11 829 ± 539	14 793 ± 544
2012.04110	54 491 ± 885	74 725 ± 1022	79 151 ± 1 352
2014.04110	17 302 ± 514	22 026 ± 578	27 683 ± 773
2017.04110	8 547 ± 427	71 053 ± 1157	74 167 ± 1 233
2018.04110	4 184 ± 105	7 606 ± 380	13 549 ± 394

Table 2.(Continued)

Time (Years)	T_r^{Max} (s)	T_d^{Max} (s)	T_t^{Max} (s)
2019.04110	13 230 ± 492	31 069 ± 749	32 485 ± 896
2019.04110	4 594 ± 115	7 827 ± 391	9 783 ± 408
2020.04110	12 056 ± 554	40 619 ± 832	52 675 ± 999

Choosing homogeneously 47 different time intervals of one month between 1976 and 2022, we separately derived 47 OPEA models by the flares in the X-ray data collected by the GOES satellites. Then, computing the model parameters and determining their variations via time, we found a variation beyond our expectations. As seen from the top panel of Fig. 3, the *Plateau* values are decreasing steadily from 1976 to 2022. This time interval corresponds to more than 4 full Solar Cycles. In addition to the *Plateau*, the y_0 parameter also exhibits a very similar variation. The y_0 parameter is the equivalent duration of the lowest flare energies that can be observed on a star within technical limits. Therefore, a steady decrease in the energies of both the biggest and smallest flares indicates a long-term variation in the flare processes observed in the Sun during this time interval.

At this point, someone may think that there may be a decrease in sensitivity of GOES detectors over time, which will vary the energies obtained. However, there are three basic proofs that the decreases in the energy limits are not related to any technical sensitivity variation. Firstly, although different satellites have been used over the years, their detectors have exactly the same technical features and structure in all satellites (Garcia 1994). Because of this, the data accumulated simultaneously by more than one satellite give the same numerical values. Secondly, flare equivalent duration are calculated using the Least Squares Method with Equation (1). Since Equation (1) includes a normalisation in itself, it eliminates almost all numerical level differences caused possibly due to detectors. Thirdly, the variation seen in *Span* values is presented in the bottom panel of Fig. 3. *Span* value is the difference between *Plateau* and y_0 that means it is a difference between the highest and lowest flare energies. As it is seen from Fig. 3, *Span* value is in a trend to decrease via time, which means that the dominant decrease is in the energies of the biggest flares. Therefore, the variations caused due to the stellar itself rather than any instrumental sensitivity variation.

However, in the literature from Dal & Evren (2011) to Yoldaş & Dal (2021), almost no findings are obtained whether the OPEA model of a star has varied over the years. In the literature, Leto et al. (1997) showed that the flare frequency of EV Lac exhibited a regular increasing trend over a 10-yr period, but this variation is related to the number of flares observed per unit time rather than the variation in the energy of the flares exhibited by a star.

Considering the first results obtained by Yoldaş & Dal (2023) over 4 one-month time intervals taken with an average of 5–6 yr apart, solar flare energy levels follow a different path from the 11-yr cyclical behaviour. Indeed, using the regression calculations by depending on the Least Squares Method in SPSS V17.0 (Green et al. 1996), we obtained a variation from 1976 to 2022, which is seen in Fig. 3. This variation shows that the *Plateau* follows a linear trend decreasing over time. It means that although the Sun

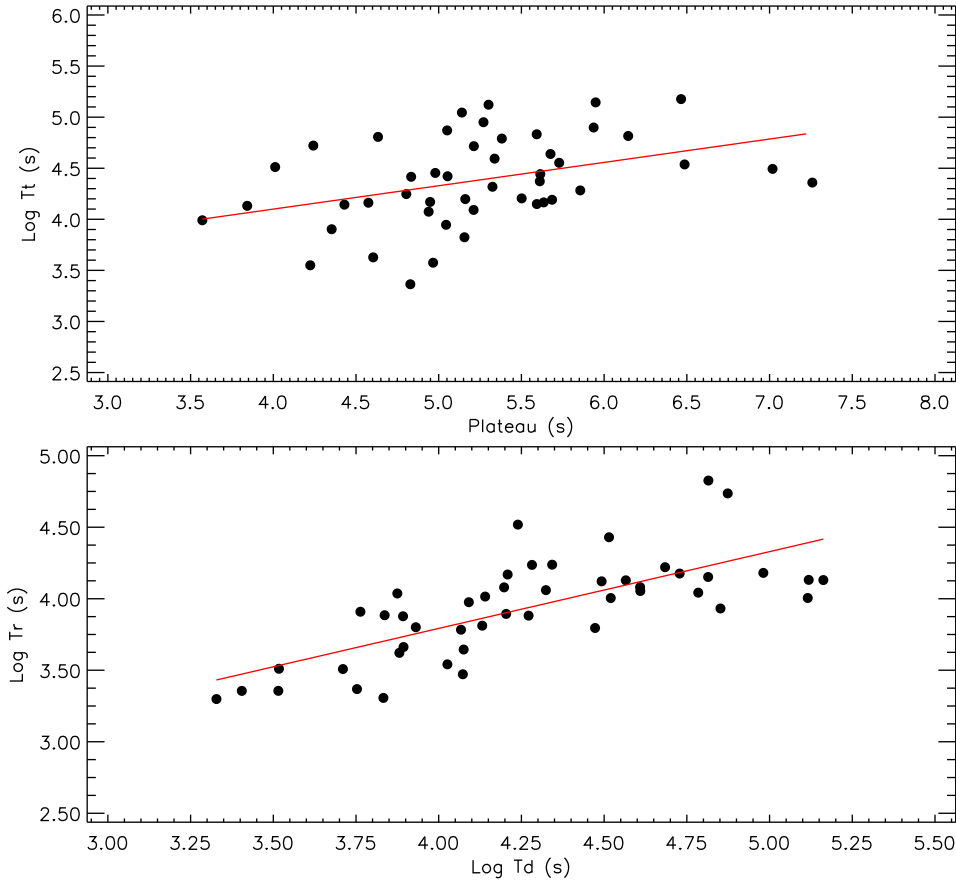


Figure 5. The variation of the longest flare duration obtained from the models versus the Plateau parameter obtained from 47 separate OPEA Models derived with X-ray data in the 0.5–4.0 Å (short channel) wavelength range taken from the GOES database is presented in the upper panel. The longest flare rise time variation via the longest flare decay time is presented in the lower panel. In the figure, the filled circles represent the timescales, while the straight line shows the linear fit.

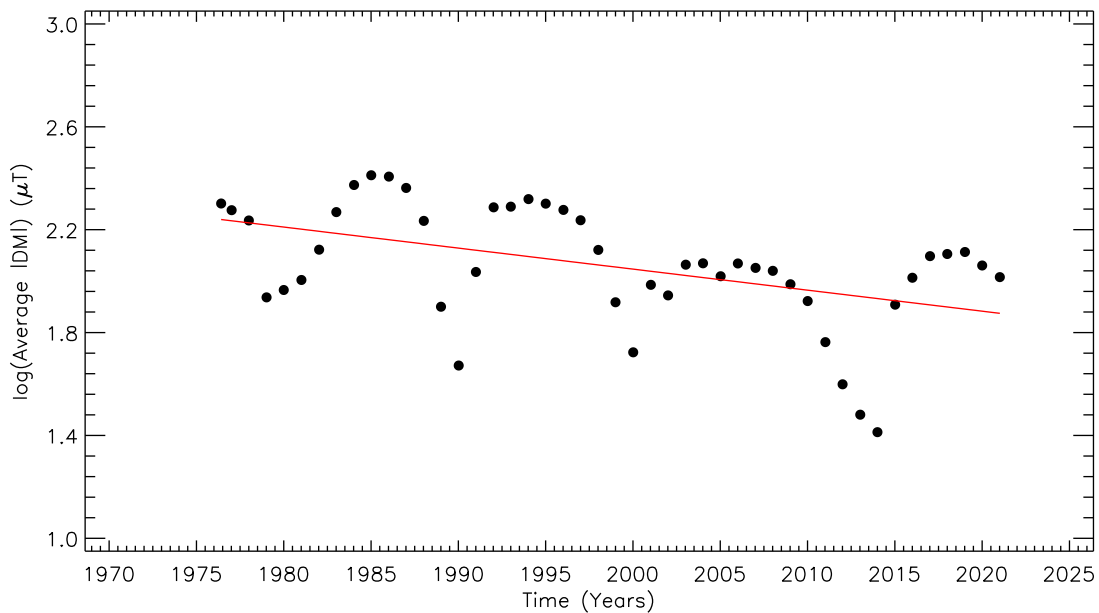


Figure 6. Using the absolute dipole moment ($|DM|$) data found in the WSO database, which are calculated with the data of the magnetic field measured between the geographical $+55^\circ / +90^\circ$ North latitudes and $-55^\circ / -90^\circ$ South latitudes of the Sun, the variation of the Average Dipole Moment (averaged $|DM|$) obtained for each month in which the OPEA model was created is shown versus time. In the figure, the filled circles represent the measurements, while the straight line shows the linear fit.

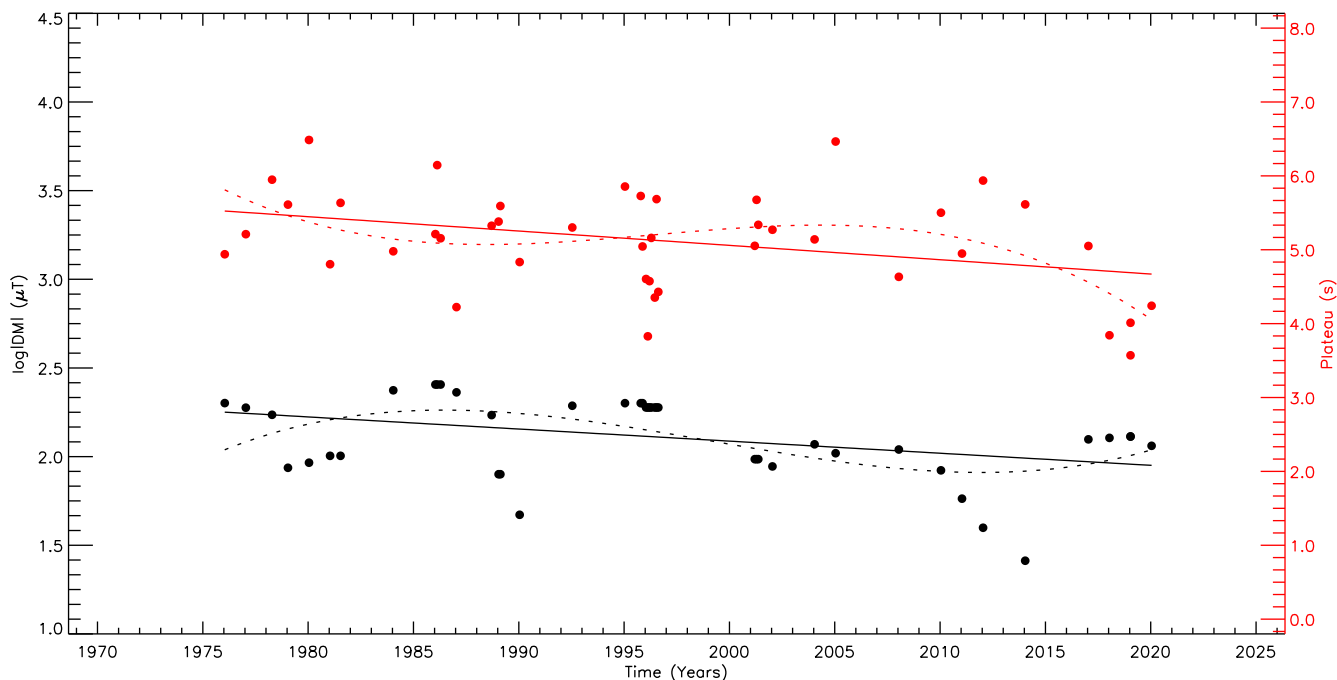


Figure 7. The variations of both the *Plateau* parameter of 47 different OPEA models and the monthly magnetic dipole moment ($|DM|$) average via time are shown. In figure, the filled red circles represent the *Plateau* parameters, while the filled black circles show the monthly magnetic dipole moment averages. The straight lines show the linear fits, while the dotted lines represent the 3-degree polynomial fits used to be able to indicate the variation seen out of linear trend.

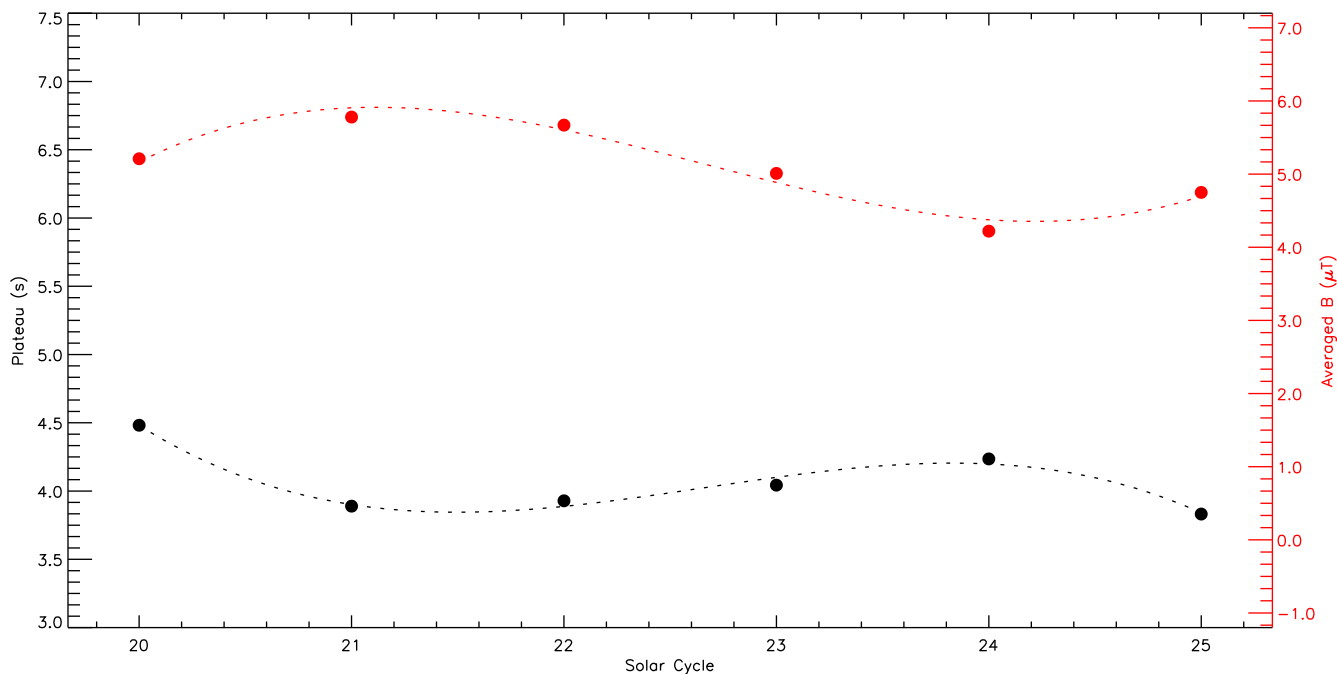


Figure 8. The cycle to cycle variation of the Solar magnetic field from the 20th Solar Activity Cycle to the 25th Cycle is compared with the variation of the *Plateau* parameter computed from the OPEA models derived separately for each cycle. In figure, the filled black circles represent the *Plateau* values, while the filled red circles show the averaged magnetic field measurements. The curves represent the 3-degree polynomial fits used to be able to indicate the variation seen out of linear trend.

exhibits flare activity at almost every energy level over the years, there is a significant decrease in solar flare energies from 1976 to 2022. In a way, this indicates that the saturation level of solar flare activity decreased over time in this years.

Considering that a flare event occurs as a result of the interaction of magnetic field and plasma, there are very few basic parameters that determine the flare energy (Gershberg 2005; Benz 2008). According to the standard magnetic reconnection model developed by Petschek (1964), these parameters are *Alfvén* velocity (v_A), magnetic field intensity (B), plasma electron density (n_e) and the emissivity of the plasma (R) (a parameter related to n_e) and the total thermal energy (E_{th}) (van den Oord & Barstow 1988; van den Oord, Mewe & Brinkman 1988). The total thermal energy (E_{th}) depends on the magnetic energy, defined as $B^2/8\pi$. As a result, a flare energy depends mainly on two parameters, which are n_e and B .

6.2 Solar flares timescales

In the OPEA models, it is seen that the *Half – Time* of these models increases by increasing *Plateau* value. The *Half – Time* duration is the theoretical shortest flare duration among the flares, whose flare energies reaches the *Plateau* level in a flare-set for which the OPEA model was derived. As can be seen from Fig. 4, there are different *Half – Time* times in almost every OPEA model. It means that the shortest flare times required to reach maximum energy vary in the case of the flares occurring over a certain period of time. In some periods, it seems that a flare must last at least 5 000 s in order to reach saturation level, while sometimes the flare can reach a flare saturation level with a total duration of 1 000 s. However, Fig. 4 also reveals that the *Half – Time* time does not vary randomly. The *Half – Time* values increase linearly while the flare energies are reaching higher energy levels.

Therefore, it becomes clear that the variation in the flare total times (T_t) should also be examined. In the study conducted by Reep & Knizhnik (2019) on the X-ray flux and durations of solar flares, it is stated that they did not find any relationship between the durations of solar X-ray flares and other fundamental flare parameters such as thermal energy, peak temperature, peak EM, peak flux, ribbon area, or magnetic flux. On the other hand, in this study, as seen in the upper panel of Fig. 5, we found that the total flare times (T_t) also increase partially, while the energies increase in a flare set. However, the flare total time (T_t) is equal to the sum of the durations of two separate special flare phases. These are flare rise time (T_r) and flare decay time (T_d). Comparing these two flare timescales with each other indicates that there is a linear relationship between the two, as seen in the bottom panel of Fig. 5. However, if the figure is examined carefully, a remarkable situation will be noticed.

The flare rise times are related to the decay times by a power law, with the positive power index smaller than 1. As a result, if the decay time is equal to 3.5 ($\log T_d = 3.5$) in a logarithmic scale for a model, the rise time is also equal to 3.5 ($\log T_r = 3.5$) in a logarithmic scale. However, the decay time is equal to 5.25 ($\log T_d = 5.25$) in a logarithmic scale for a model, the rise time is also equal to 4.5 ($\log T_r = 4.5$) in a logarithmic scale. It indicates that flare rise and decay times are generally equal to each other for the models derived over the low-energy and short-duration flares (the models on the left side of the figure). These type flares are generally called ‘slow flares’ in the literature (Kunkel 1967; Haro & Parsamian 1969; Osawa et al. 1968; Gurzadian 1988; Gershberg

2005). On the other hand, in the case of the models derived over the flares with relatively high energies and long durations (the models on the right side of the figure) generally have a short rise time but a long decay time. In the literature, these type flares are generally called ‘fast flares’ (Kunkel 1967; Haro & Parsamian 1969; Osawa et al. 1968; Gurzadian 1988; Gershberg 2005). In the solar case, such flares are known as ‘two ribbon flares having very high-energies, where the magnetic reconnection is very dominant (Rodono 1990; Gershberg 2005; Benz & Güdel 2010). When the upper and lower panels of Fig. 5 are evaluated together, it is seen that the obtained models are in agreement with the literature, which shows the accuracy of the work done.

The flare rise time (T_r) corresponds to the part defined as the ‘impulsive phase’ in the Standard Solar Flare Model (Benz 2008; Benz & Güdel 2010; Benz 2017). However, the length of the flare decay time is related to the magnetic loop height and geometry to which the flare event is associated (Reeves & Warren 2002; Imanishi et al. 2003; Török & Kliem 2004; Favata et al. 2005; Pandey & Singh 2008).

Describing the half length of loop as L , Reeves & Warren (2002) defined the cooling timescale as:

$$\tau_c = (4 \times 10^{-10}) \times \frac{n_e \times L^2}{T_e^{5/2}} \quad (3)$$

where T_e and n_e are the electron temperature and density of magnetic loop. Similarly, van den Oord & Mewe (1989), Serio et al. (1991), Favata et al. (2005), and Pandey & Singh (2008) described the relation between the flare timescale and the half length of loop as:

$$L = \frac{\tau_{th} \times \sqrt{T_{pk}}}{3.7 \times 10^{-4}} \quad (4)$$

where τ_{th} is effective decay timescale and T_{pk} is the plasma temperature in the magnetic loop peak in units of 10^7 K. In the definitions made by these authors with different approaches, the magnetic loop height always seems to be related to the flare decay times. In addition, Imanishi et al. (2003) report that small timescales are associated with small half length of magnetic loop (L) in a flare event.

On the other hand, van den Oord & Barstow (1988) defines the decay time as $T_d \propto E_{th}/R$, which they define as the radiative loss timescale. Considering that the parameter R also depends on the electron density (n_e), it can be seen that the flare decay time (T_d) is also closely related to the magnetic field intensity (B) and electron density (n_e).

Thus, the linear relationships between the *Plateau* and flare timescales (*Half – Time*, T_r , T_d) in Figs. 4 and 5 get meaning. The flare energy and its loop geometry depend on the magnetic field strength (B) of the loop and the electron density (n_e) in the environment.

6.3 Plateau and dipole moment relationship

In the literature, there are numerous studies examining the relationship between the Sun’s magnetic field structure and the configuration changes associated with its flare activity (Reep & Knizhnik 2019; Qiu 2021). When each flare event is individually evaluated, solar flare activity is generally associated with the magnetic field structures in the active regions on the solar surface. In those studies, no strong correlation has been found between the magnetic fields measured at the solar poles and flare-like structures in the

active regions. However, when we look at the statistical behaviour of the solar activity structures, particularly flares, we reach interesting conclusions. In this study, where the flare data spread over many years is statistically examined, we report a correlation finding between the solar X-ray flares and the solar polar magnetic structures.

In order to examine how the variation of the *Plateau* level, which is an indicator of the saturation levels of solar flare energies, is affected by the magnetic field (B) and electron density (n_e), there is a need to measure these two solar atmospheric parameters between 1976 and 2022. Although atmospheric average magnetic field (B) measurements have been made regularly, both directly on the solar surface and indirectly since the 1950s, the long-term regular measurements of electron density (n_e) in the solar atmosphere are not available in the literature.

However, MWO and WSO measurements, which have been made quite regularly and with a very small error of 5 m Tesla since the early 1970s (Svalgaard et al. 2005), have enabled us to know more about the solar magnetic field than the electron density (n_e). It is well known in the literature that the magnetic field intensity measured in the solar geographical polar regions decreases (Ghizaru et al. 2010).

When examining carefully the variation of the monthly average magnetic dipole moment in the one-month periods for which the flares for which the OPEA model was created rather than the annual magnetic dipole moment average for whole year in which one OPEA model is created at least, two important results are revealed. First of all, as it is seen in Fig. 7, the magnetic dipole moment ($|DM|$) decreases over time, just like Ghizaru et al. (2010) have suggested. What is noteworthy here is that both *Plateau* and $|DM|$ decrease by following an isodirectional trend with a very similar slope. Primarily Svalgaard et al. (2005) and Ghizaru et al. (2010) point out that the solar magnetic dipole moment values measured between the geographical $+55^\circ / +90^\circ$ Northern latitudes and $-55^\circ / -90^\circ$ Southern latitudes are decreasing steadily. The effect of this decreasing clearly shows itself in general energy levels of the flares.

Here an important similarity is noticeable in the details. In both Figs. 3 and 7, while the *Plateau*, y_0 and $|DM|$ variations in measurements are represented by a linear model, it is seen that all of them are also represented by a 3rd degree polynomial. It is not currently possible to define a physical process for these polynomial representations. The reason why we also need to fitted the variations by a polynomial function is that when *Plateau* and y_0 are represented by a linear model in Fig. 3, the data on the left side of both parameters tend to accumulate below the linear line, and the data on the right side tend to accumulate above it. However, this situation is exactly the opposite in the $|DM|$ variation.

On the other hand, these two findings show themselves much more strikingly when tested with the solar magnetic measurements obtained indirectly by van Driel-Gesztelyi & Owens (2020). As seen in Fig. 8, both the solar magnetic field (B) variation determined by van Driel-Gesztelyi & Owens (2020) as an average value for each solar cycle, from the 20th to the 25th cycle and the *Plateau* value variation determined from the general OPEA models derived for each cycle are perfect mirror images of each other. The average magnetic field obtained by van Driel-Gesztelyi & Owens (2020) also decreases steadily as well as the *Plateau*. As a result, the ‘sine-like’ variation indicated by the 3rd degree polynomial in monthly models reveals itself much more clearly in these cyclic values. The findings obtained from Figs. 7 and 8 show that

the solar flare energies generally vary directly depending on the magnetic field.

Conclusion

Within the scope of this study, we have shown that there is a decrease in the general energy level of X-ray flares observed on the Sun from 1976 to 2022, and this decrease occurs due to the variation in the magnetic field intensity measured from the solar polar regions. However, it is noticed that there is also a secondary variation that seems to be suppressed in addition to the decreasing linear trend. It is a known fact that flare energy is tightly dependent on the magnetic field (B) and electron density (n_e). However, although this study clearly showed the effect of the magnetic field (B) on flare energies in the long term, no physical inference is made as to what caused the sinusoidal variation in both the magnetic field and the energies. What prevents us from making a definitive approach here is the lack of data on how the electron density (n_e), which is a known fact to have an effect on energies, has changed over the years. If such data can be created in the coming years, this issue will also become clear.

Acknowledgements. We thank the referee for useful comments that have contributed to the improvement of the paper. We would like to express our gratitude to the Ege University Observatory for providing us with software and technical support throughout this study. This study is continued within the scope of the study entitled ‘Determination of X-ray flare behaviour in solar activity with the OPEA model’ carried out in the Graduate School of Natural and Applied Science of Ege University.

Data Availability Statement. The data underlying this article will be shared on reasonable request to the corresponding author.

References

- Arlt, R. 2011, *AN*, **332**, 805
- Aulanier, G., Démoulin, P., Schrijver, C. J., Janvier, M., Pariat, E., & Schmieder, B. 2013, *A&A*, **549**, A66
- Babcock, H. D. 1959, *ApJ*, **130**, 364
- Babcock, H. W., & Babcock, H. D. 1955, *ApJ*, **121**, 349
- Benz, A. O. 2008, *LRSP*, **5**, 1
- Benz, A. O. 2017, *LRSP*, **14**, 2
- Benz, A. O., & Güdel, M. 2010, *ARA&A*, **48**, 241
- Berdugina, S. V. 2005, *LRSP*, **2**, 8
- Bertello, L., Pevtsov, A. A., & Ulrich, R. K. 2020, *ApJ*, **897**, 181
- Carrington, R. C. 1859, *MNRAS*, **20**, 13
- Clark, D. H., & Stephenson, F. R. 1978, *QJRAS*, **19**, 387
- Cliver, E. W., & Svalgaard, L. 2004, *SoPh*, **224**, 407
- D’Agostino, R. B., & Stephens, M. A. 1986, *Goodness-of-fit techniques, Statistics: Textbooks and Monographs*, eds. R. B. D’Agostino & M. A. Stephens (New York: Dekker), 367–421
- Dal, H. A. 2020, *MNRAS*, **495**, 4529
- Dal, H. A., & Evren, S. 2010, *AJ*, **140**, 483
- Dal, H. A., & Evren, S. 2011, *AJ*, **141**, 33
- Dal, H. A., & Yoldaş, E. 2023, *Ap&SS*, **368**, 43
- Dawson, B., & Trapp, R. 2004, *Basic & Clinical Biostatistics 4/E* (EBOOK). LANGE Basic Science (McGraw-Hill Education), <https://books.google.com.tr/books?id=p6hu-qU2zpsC>
- Dierckxsens, M., Patsou, I., Tziotziou, K., Marsh, M., Lygeros, N., Crosby, N., Dalla, S., & Malandraki, O. 2013, in *EGU General Assembly Conference Abstracts*, EGU2013–8865
- Dikpati, M., de Toma, G., Gilman, P. A., Corbard, T., Rhodes, E. J., Haber, D. A., Bogart, R. S., & Rose, P. J. 2004, in *American Astronomical Society Meeting Abstracts #204*, 53.05

- Favata, F., Flaccomio, E., Reale, F., Micela, G., Sciortino, S., Shang, H., Stassun, K. G., & Feigelson, E. D. 2005, *ApJS*, **160**, 469
- Garcia, H. A. 1994, *SoPh*, **154**, 275
- Gershberg, R. E. 1972, *Ap&SS*, **19**, 75
- Gershberg, R. E. 2005, *Solar-Type Activity in Main-Sequence Stars* (New York: Springer), 53. doi: [10.1007/3-540-28243-2](https://doi.org/10.1007/3-540-28243-2).
- Ghizaru, M., Charbonneau, P., & Smolarkiewicz, P. K. 2010, *ApJ*, **715**, L133
- Gilman, P. A. 2000, *ApJ*, **544**, L79
- Gilman, P. 2020, in *AGU Fall Meeting Abstracts*, SH006–01
- Green, S. B., Salkind, N. J., & Jones, T. M. 1996, *Using SPSS for Windows: Analyzing and Understanding Data* (1st edn.; Upper Saddle River, NJ, USA: Prentice Hall PTR)
- Gurzadian, G. A. 1988, *ApJ*, **332**, 183
- Haro, G., & Parsamian, E. 1969, *BOTT*, **5**, 45
- Hathaway, D. H. 2010, *LRSP*, **7**, 1
- Hathaway, D. H. 2015, *LRSP*, **12**, 4
- Hodgson, R., 1859, *MNRAS*, **20**, 15
- Imanishi, K., Nakajima, H., Tsujimoto, M., Koyama, K., & Tsuboi, Y. 2003, *PASJ*, **55**, 653
- Kunkel, W. E. 1967, PhD thesis, University of Texas, Austin
- Leto, G., Pagano, I., Buemi, C. S., & Rodono, M. 1997, *A&A*, **327**, 1114
- Maehara, H., et al. 2012, *Natur*, **485**, 478
- McCracken, K. G., Smart, D. F., Shea, M. A., & Dreschhoff, G. A. M. 2001, in *International Cosmic Ray Conference*, 3209
- Motorina, G. G., Lysenko, A. L., Anfinogentov, S. A., & Fleishman, G. D. 2020, *Ge&Ae*, **60**, 929
- Motulsky, H. 2007, *GraphPad Software*, **31**, 39
- Mursula, K., & Ulich, T. 1998, *GeoRL*, **25**, 1837
- Osawa, K., Ichimura, K., Noguchi, T., & Watanabe, E. 1968, *TokAB*, **188**, 2205
- Pandey, J. C., & Singh, K. P. 2008, *MNRAS*, **387**, 1627
- Petschek, H. E. 1964, in Vol. 50 (NASA Special Publication), 425
- Qiu, J. 2021, *ApJ*, **909**, 99
- Reep, J. W., & Knizhnik, K. J. 2019, *ApJ*, **874**, 157
- Reeves, K. K., & Warren, H. P. 2002, *ApJ*, **578**, 590
- Rodono, M. 1990, in Vol. 137, *Flare Stars in Star Clusters, Associations and the Solar Vicinity*, ed. L. V. Mirzozian, B. R. Pettersen, & M. K. Tsvetkov, 371
- Schaefer, B. E., King, J. R., & Deliyannis, C. P. 2000, *ApJ*, **529**, 1026
- Schrijver, C. J., et al. 2012, *JGR (Space Physics)*, **117**, A08103
- Schwabe, H. 1844, *AN*, **21**, 233
- Serio, S., Reale, F., Jakimiec, J., Sylwester, B., & Sylwester, J. 1991, *A&A*, **241**, 197
- Severny, A. B. 1971, in Vol. 43, *Solar Magnetic Fields*, ed. R. Howard, 675
- Shibata, K., & Magara, T. 2011, *LRSP*, **8**, 6
- Shibata, K., & Yokoyama, T. 2002, *ApJ*, **577**, 422
- Shibata, K., et al. 2013, *PASJ*
- Shibayama, T., et al. 2013, *ApJS*
- Skumanich, A. 1972, *ApJ*, **171**, 565
- Spanier, J., & Oldham, K. B. 1987, *An Atlas of Functions* (Bristol, PA, USA: Taylor & Francis/Hemisphere)
- Strassmeier, K. G. 2009, *A&A Rev.*, **17**, 251
- Svalgaard, L., Duvall, T. L. J., & Scherrer, P. H. 1978, *SoPh*, **58**, 225
- Svalgaard, L., Cliver, E. W., & Kamide, Y. 2005, *GeoRL*, **32**, L01104
- Török, T., & Kliem, B. 2004, *PADEU*, **14**, 165
- Ulrich, R. K., Evans, S., Boyden, J. E., & Webster, L. 2002, *ApJS*, **139**, 259
- van Driel-Gesztelyi, L., & Owens, M. J. 2020, *Solar Cycle*, [10.1093/acrefore/9780190871994.013.9](https://doi.org/10.1093/acrefore/9780190871994.013.9), <https://oxfordre.com/physics/view/10.1093/acrefore/9780190871994.001.0001/acrefore-9780190871994-e-9>
- van den Oord, G. H. J., & Barstow, M. A. 1988, *A&A*
- van den Oord, G. H. J., & Mewe, R. 1989, *A&A*, **213**, 245
- van den Oord, G. H. J., Mewe, R., & Brinkman, A. C. 1988, *A&A*
- Weiss, N. O., & Tobias, S. M. 2000, in Vol. 11, *Solar Variability and Climate*, ed. E. Friis-Christensen, C. Fröhlich, J. D. Haigh, M. Schüssler, & R. Von Steiger, 99, [10.1007/978-94-010-0888-4_10](https://doi.org/10.1007/978-94-010-0888-4_10)
- White, S. M., Bastian, T. S., Bradley, R., Parashare, C., & Wye, L. 2005, in *Astronomical Society of the Pacific Conference Series Vol. 345, From Clark Lake to the Long Wavelength Array: Bill Erickson's Radio Science*, N. Kassim, M. Perez, W. Junor, P. Henning, 176
- Wittmann, A. D., & Xu, Z. T. 1987, *PPMtO*, **6**, 233
- Yoldaş, E., & Dal, H. A. 2016, *PASA*, **33**, e016
- Yoldaş, E., & Dal, H. A. 2017, *PASA*, **34**, e060
- Yoldaş, E., & Dal, H. A. 2021, *RMxAA*, **57**, 39
- Yoldaş, E., & Dal, H. A. 2022, *MNRAS*, **517**, 1937
- Yoldaş, E., & Dal, H. A. 2023, *A&C*, **45**, 100756